



Article

# Photocatalytic Degradation of Diclofenac Using Al<sub>2</sub>O<sub>3</sub>-Nd<sub>2</sub>O<sub>3</sub> Binary Oxides Prepared by the Sol-Gel Method

José Eduardo Casillas <sup>1</sup>, Jorge Campa-Molina <sup>2</sup>, Francisco Tzompantzi <sup>3</sup>,  
Gregorio Guadalupe Carbajal Arízaga <sup>4</sup> , Alejandro López-Gaona <sup>3</sup>, Sandra Ulloa-Godínez <sup>2</sup>,  
Mario Eduardo Cano <sup>1</sup>  and Arturo Barrera <sup>1,\*</sup>

<sup>1</sup> Departamento de Ciencias Básicas, Centro Universitario de la Ciénega, Universidad de Guadalajara, Av. Universidad, No. 1115, Ocotlán C.P. 47820, Jalisco, Mexico; duartcasillas88@gmail.com (J.E.C.); meduardo2001@hotmail.com (M.E.C.)

<sup>2</sup> Departamento de Electrónica, Universidad de Guadalajara, Marcelino García Barragán 1422, Guadalajara C.P. 44430, Jalisco, Mexico; jcampamolina@gmail.com (J.C.-M.); sago2063@gmail.com (S.U.-G.)

<sup>3</sup> Departamento de Química, Universidad Autónoma Metropolitana—Iztapalapa, San Rafael Atlixco 189, Ciudad de México C.P. 09340, Mexico; fjtz@xanum.uam.mx (F.T.); gaby@xanum.uam.mx (A.L.-G.)

<sup>4</sup> Departamento de Química, Universidad de Guadalajara, Marcelino García Barragán 1422, Guadalajara C.P. 44430, Jalisco, Mexico; gregoriocarbjal@yahoo.com.mx

\* Correspondence: arturo.barrera@cuci.udg.mx or arturoobr2003@yahoo.com.mx

Received: 31 January 2020; Accepted: 10 March 2020; Published: 16 March 2020



**Abstract:** This paper reports the sol-gel synthesis of Al<sub>2</sub>O<sub>3</sub>-Nd<sub>2</sub>O<sub>3</sub> (Al-Nd-*x*; *x* = 5%, 10%, 15% and 25% of Nd<sub>2</sub>O<sub>3</sub>) binary oxides and the photodegradation of diclofenac activated by UV light. Al-Nd-based catalysts were analyzed by N<sub>2</sub> physisorption, XRD, TEM, SEM, UV-Vis and PL spectroscopies. The inclusion of Nd<sub>2</sub>O<sub>3</sub> in the aluminum oxide matrix in the 10–25% range reduced the band gap energies from 3.35 eV for the  $\gamma$ -Al<sub>2</sub>O<sub>3</sub> to values as low as 3.13–3.20 eV, which are typical of semiconductor materials absorbing in the UV region.  $\gamma$ -Al<sub>2</sub>O<sub>3</sub> and Al-Nd-*x* binary oxides reached more than 92.0% of photoconverted diclofenac after 40 min of reaction. However, the photocatalytic activity in the diclofenac degradation using Al-Nd-*x* with Nd<sub>2</sub>O<sub>3</sub> contents in the range 10–25% was improved with respect to that of  $\gamma$ -Al<sub>2</sub>O<sub>3</sub> at short reaction times. The diclofenac photoconversion using  $\gamma$ -Al<sub>2</sub>O<sub>3</sub> was 63.0% at 10 min of UV light exposure, whereas Al-Nd-15 binary oxide reached 82.0% at this reaction time. The rate constants determined from the kinetic experiments revealed that the highest activities in the aqueous medium were reached with the catalysts with 15% and 25% of Nd<sub>2</sub>O<sub>3</sub>, and these compounds presented the lowest band gap energies. The experimental results also demonstrated that Nd<sub>2</sub>O<sub>3</sub> acts as a separator of charges favoring the decrease in the recombination rate of electron-hole pairs.

**Keywords:** Al<sub>2</sub>O<sub>3</sub>-Nd<sub>2</sub>O<sub>3</sub>; sol-gel; diclofenac; photodegradation; structure; band-gap energy

## 1. Introduction

Aluminum oxide is an insulating material with band gap energy values above 5 eV [1–3]. The energy in this gap can be reduced to values as low as 2.5 eV by adjusting the content of defects on its surface [4–6]. According to previous reports, the modified surface can be considered a new phase with different properties associated to new surface chemistry and chemical activity [4–6]. We have reported that the sol-gel method is suitable to produce  $\gamma$ -Al<sub>2</sub>O<sub>3</sub> with photocatalytic activity to degrade organic pollutants in water [7–9], however it is desirable to enhance photocatalytic performance in order to reach a higher conversion in the lowest time. In earlier works, the photocatalytic activity of

$\gamma$ -Al<sub>2</sub>O<sub>3</sub> in the degradation of phenolic compounds has been improved by impregnating noble metal (PdO or Ag<sup>0</sup>) onto Al<sub>2</sub>O<sub>3</sub>-Ln<sub>2</sub>O<sub>3</sub> (Ln = Nd or Gd) binary oxides [8,10,11] or by doping Al<sub>2</sub>O<sub>3</sub>-Nd<sub>2</sub>O<sub>3</sub> with the semiconducting ZnO to form Al<sub>2</sub>O<sub>3</sub>-Ln<sub>2</sub>O<sub>3</sub>-ZnO ternary oxides [9]. Although the experimental evidences demonstrated that the photocatalytic activity of  $\gamma$ -Al<sub>2</sub>O<sub>3</sub> enhances with the addition of rare earth oxides, semiconducting oxides, or noble metals, the performance against degradation of drug pollutants in water is still unknown; therefore, we proposed to study the photocatalytic degradation of diclofenac in aqueous medium catalyzed with Al<sub>2</sub>O<sub>3</sub>-Nd<sub>2</sub>O<sub>3</sub> binary oxides and the efficiency related to the Nd<sub>2</sub>O<sub>3</sub> content.

Diclofenac is an anti-inflammatory drug used frequently by human beings which is discharged into the wastewater causing further pollution in different sources of drinking water [12–14], since it is very stable against the conventional treatments of water [15,16]. The persistence in ecosystems occurs due to the low biodegradability and this is also a reason for the incomplete removal in water treatments based on microbiological activity [14–17]. Therefore, more efficient methods to eliminate this molecule are needed, and the photodegradation arises as an alternative. Then, this work studies the preparation of aluminum oxides with different contents of Nd<sub>2</sub>O<sub>3</sub> and the relationship with the photocatalytic activity to degrade diclofenac in aqueous solutions. The characterization of the binary oxides by different solid-state techniques will be presented.

## 2. Materials and Methods

### 2.1. Synthesis

The sol-gel method was selected since this procedure allows for the simultaneous formation of metal oxides [8–11]. First, a solution with a certain amount of aluminum tri-sec-butoxide (97.0%, Aldrich, St. Louis, MO, USA) and 10 mL of 2-methylpentane 2,4-diol (99.999%, JT Baker, Phillipsburg, USA) as a complexing agent was stirred in a round glass flask for 60 min while the temperature was kept at 70 °C. Thereafter, the temperature was reduced to 50 °C and mixed with a second solution prepared by dissolving neodymium acetylacetonate (99.99%, Aldrich) in toluene (99.999%, Aldrich) at 40 °C. The resulting solution was stirred at 50 °C, then, after 60 min, 10 mL of deionized water was added dropwise to promote the hydrolysis of the aluminum and neodymium reagents to produce a gel. This gel was aged by heating first at 55 °C for 2 h and then at 80 °C for 12 h. The product at this step was a powder, which was dried 110 °C for 12 h and then calcined under air atmosphere at 650 °C for 4 h. The Al<sub>2</sub>O<sub>3</sub>-Nd<sub>2</sub>O<sub>3</sub> binary oxides obtained after this process were labeled as Al-Nd-*x*, where *x* represents the mass percentage of Nd<sub>2</sub>O<sub>3</sub> in the Al<sub>2</sub>O<sub>3</sub> matrix. The content of Nd<sub>2</sub>O<sub>3</sub> was 5%, 10%, 15% and 25%.

Bare Al<sub>2</sub>O<sub>3</sub> (labeled as Al) was prepared by the same sol-gel procedure with aluminum tri-sec-butoxide, whereas the Nd<sub>2</sub>O<sub>3</sub> reference was obtained by calcining neodymium acetylacetonate at 800 °C for 5 h.

### 2.2. Solid State Characterization

Textural properties of the photocatalysts were studied by nitrogen physisorption at the saturation temperature of liquid nitrogen (−195.6 °C) with Quantachrome Autosorb equipment, model IQ. The samples were conditioned by degassing with helium at 300 °C for 5 h.

The structural property oxides were studied by powder X-ray diffraction with an STOE diffractometer, model Theta-Theta operated with Cu K $\alpha$  ( $\lambda = 0.154$  nm) radiation. The analysis was conducted in the 2 $\theta$  mode with a 2 $\theta$  step of 0.02° and collecting time of 60 s. High-resolution transmission electron microscopy (HRTEM) micrographs were acquired with a HRTEM FEI TECNAI F30 STWIN G2 microscope (Hillsboro, USA) with a power of 300 kV and a resolution of 24 nm. The morphology was studied with a scanning electron microscope (SEM) using a HRSEM Jeol 7600F microscope (Tokyo, Japan) operated with 30 kV. The chemical composition was determined with an energy dispersive X-ray spectroscopy (EDS) detector coupled to the microscope.

The absorption of UV-vis light necessary to determine the optical properties of the photocatalyst was measured with an UV-Vis CARY 300 (Varian, Victoria, Australia) spectrophotometer. The scanning was conducted with a speed of 600 nm per minute and resolution of 1 nm. The spectra were treated with the Kubelka-Munk function to determine the absorption edge and absorbance according to Equation (1), where  $E_g$  is the band gap energy,  $\alpha$  is the measured absorbance, the product  $h\nu$  corresponds to the photon energy, and B is a constant for these materials [18,19]:

$$\alpha h\nu = B(h\nu - E_g)^2 \quad (1)$$

From this equation the  $(\alpha h\nu)^{1/2}$  and  $h\nu$  values are plotted, and the linear part is extrapolated to determine the band gap energy. This relationship is known as the Tauc graph [20].

The photoluminescence spectra were obtained with a Fluorescence Varian Cary eclipse spectrophotometer using an excitation wavelength of 270 nm.

### 2.3. Photocatalytic Activity

The degradation of diclofenac was selected as the model to study the photocatalytic activity of the oxides, and the reactions were conducted in round bottom cylindrical glass with 1 L of capacity assembled to a glass jacket with double wall. The photodegradation of diclofenac (99.9%, Sigma-Aldrich) was studied with 80 ppm aqueous solutions. Before the reactions, this solution was bubbled with air during 12 h, and then 200 mL was transferred to the cylindrical glass and mixed with 200 mg of the Al-Nd- $x$  sample representing a concentration of 1 mg of catalyst  $\text{mL}^{-1}$ . The diclofenac solution was stirred and air was injected at a rate of 1  $\text{mL s}^{-1}$ , then a UV lamp (UVP products) emitting a 254 nm light with irradiance of 4400  $\mu\text{W cm}^{-2}$  was introduced into the diclofenac solution. The photodegradation was followed as a function of time; for this, aliquots were removed every 5 min using a filter for the first 20 min, thereafter, the aliquots were collected at intervals of 10 min for a period of 60 min. The samples were analyzed by UV-Vis spectroscopy in a CARY 300 spectrophotometer. The quantification of diclofenac was based on the absorption at 275 nm and the kinetic was studied for a total period of 80 min of irradiation;  $\gamma\text{-Al}_2\text{O}_3$  and  $\text{Nd}_2\text{O}_3$  were used as references. As commonly reported for photodegradation of organic compounds in aqueous medium [21,22], the data were treated with the pseudo first-order equation of the Langmuir-Hinshelwood model:

$$\text{Ln}(C_0/C) = k_{\text{app}}t \quad (2)$$

## 3. Results and Discussion

### 3.1. Textural Properties of Photocatalysts

The textural properties of pure  $\gamma\text{-Al}_2\text{O}_3$  and Al-Nd- $x$  binary oxides are shown in Figure 1. Bare  $\gamma\text{-Al}_2\text{O}_3$  shows a BET specific surface area ( $S_{\text{BET}}$ ) of 250  $\text{m}^2 \text{g}^{-1}$  (Figure 1A). The  $S_{\text{BET}}$  of  $\gamma\text{-Al}_2\text{O}_3$  increased with neodymium oxide concentration to reach a maximum  $S_{\text{BET}}$  (266.0  $\text{m}^2 \text{g}^{-1}$ ) in the Al-Nd-10 sample. The increment of the  $S_{\text{BET}}$  value indicates that neodymium oxide enhances the textural features of  $\gamma\text{-Al}_2\text{O}_3$  at low  $\text{Nd}_2\text{O}_3$  concentration ( $\leq 10\%$ ). A drop in the  $S_{\text{BET}}$  was observed at higher  $\text{Nd}_2\text{O}_3$  concentration ( $>10\%$ ), reaching a  $S_{\text{BET}} = 205.0 \text{ m}^2 \text{g}^{-1}$  in the Al-Nd-25 binary oxide. The pronounced drop in the  $S_{\text{BET}}$  of binary oxides at high  $\text{Nd}_2\text{O}_3$  concentration might be due to the blocking of the alumina porous structure by the presence of  $\text{Nd}_2\text{O}_3$  nanoparticles that are highly dispersed among the alumina agglomerates. The specific mesopore volume of  $\gamma\text{-Al}_2\text{O}_3$  ( $V_{\text{meso}} = 1.1 \text{ cm}^3 \text{g}^{-1}$ ) decreased with the  $\text{Nd}_2\text{O}_3$  concentration reaching a  $V_{\text{meso}} = 0.5 \text{ cm}^3 \text{g}^{-1}$  in the Al-Nd-25 binary oxide (Figure 1B), whereas the specific micropore volume was approximately constant ( $V_{\text{micro}} = 0.3 \text{ cm}^3 \text{g}^{-1}$ ) for all the materials. The average pore size (APS) of Al-Nd- $x$  binary oxide also decreased with neodymium oxide concentration from 12.0 nm in the bare  $\gamma\text{-Al}_2\text{O}_3$  to 6.0 nm in the Al-Nd-25 sample (Figure 1C).

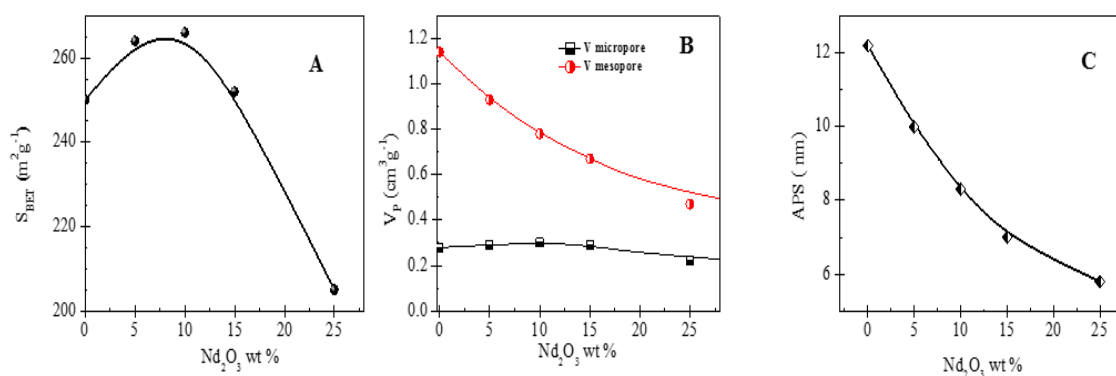


**Figure 1.** (A) BET specific surface area, (B) specific micropore and mesopore volume, and (C) average pore size of the Al-Nd-*x* binary oxides.

### 3.2. Crystalline Structure of Catalysts

Figure 2 shows the XRD patterns of the Al-Nd-*x* binary oxides and the references Al<sub>2</sub>O<sub>3</sub> and Nd<sub>2</sub>O<sub>3</sub>. The aluminum oxide phase corresponded to  $\gamma$ -Al<sub>2</sub>O<sub>3</sub> identified with the pattern recorded in the JCPDS card 10-0425, whilst the neodymium oxide sample contained the A-type hexagonal structure with cell parameters  $a = 3.827 \text{ \AA}$  and  $c = 5.991 \text{ \AA}$  (JCPDS card: 75-2255) [23]. Regarding the binary oxides, the patterns presented diffraction peaks at  $2\theta$  angles between  $31.9^\circ$  and  $66.4^\circ$  corresponding only to the  $\gamma$ -Al<sub>2</sub>O<sub>3</sub> phase (JCPDS card: 10-0425). This observation suggests that small Nd<sub>2</sub>O<sub>3</sub> nanoparticles are highly dispersed among the  $\gamma$ -Al<sub>2</sub>O<sub>3</sub> agglomerates, which are below the limit of detection by XRD. Additionally, the reflections associated to the  $\gamma$ -Al<sub>2</sub>O<sub>3</sub> phase decrease as the concentration of Nd<sub>2</sub>O<sub>3</sub> increases, indicating a reduction of the crystalline quality of the alumina structure. It seems that a high Nd<sub>2</sub>O<sub>3</sub> concentration ( $>10 \text{ wt\%}$ ) in the Al-Nd-*x* binary oxide causes a disorder in the  $\gamma$ -Al<sub>2</sub>O<sub>3</sub> structure, leading to a more disordered material.

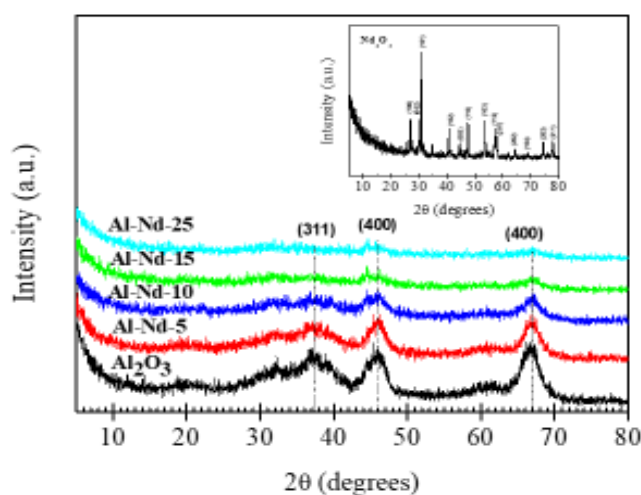


**Figure 2.** XRD patterns of  $\gamma$ -Al<sub>2</sub>O<sub>3</sub> and Al-Nd-*x* binary oxides prepared by the sol-gel method.

The HRTEM micrograph was useful to identify the presence of the Nd<sub>2</sub>O<sub>3</sub> phase with the A-type hexagonal structure. Figure 3A presents clear crystalline regions with defined grain boundaries. Additionally, the square inset in the same figure contains fringes of diffraction points; therefore, the existence of well-crystallized Nd<sub>2</sub>O<sub>3</sub> is confirmed. The interplanar distance ( $d_{hkl} = 0.32 \text{ nm}$ ) identified in the inset corresponds to the crystalline plane  $hkl(100)$  of Nd<sub>2</sub>O<sub>3</sub> of the A-type hexagonal structure (24-0779 JCPDS). Furthermore, the HRTEM micrograph of the Al-Nd-15 sample (Figure 3B) corroborates the presence of nano-crystalline domains of Nd<sub>2</sub>O<sub>3</sub> denoted by dark regions of approximately 8.0–10.0

nm in size, which are well mixed with the alumina agglomerates forming a highly disordered material at this high  $\text{Nd}_2\text{O}_3$  concentration.

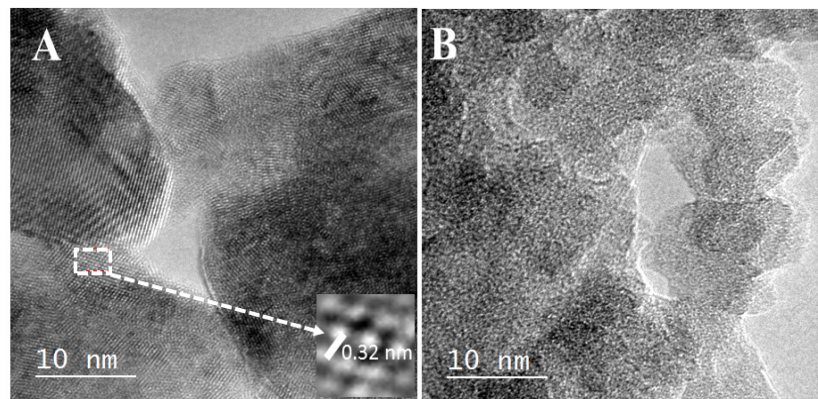


**Figure 3.** High-resolution transmission electron microscopy (HRTEM) micrographs of (A)  $\text{Nd}_2\text{O}_3$  and (B) Al-Nd-15 binary oxide.

The high dispersion of small  $\text{Nd}_2\text{O}_3$  nanoparticles among the  $\gamma\text{-Al}_2\text{O}_3$  agglomerates is confirmed by the EDS image of the Al-Nd-15 binary oxide (Figure 4A) and by the mapping of the element Nd  $M\alpha$  of the sample (Figure 4B) exhibiting a high dispersion of  $\text{Nd}_2\text{O}_3$  nanoparticles denoted by tiny spots in color blue over big  $\gamma\text{-Al}_2\text{O}_3$  agglomerates of approximately  $200\ \mu\text{m}$  in size. It seems that 15 wt.% of  $\text{Nd}_2\text{O}_3$  is the limit concentration in order to obtain a high dispersion of small  $\text{Nd}_2\text{O}_3$  particles among the alumina agglomerates, although a disordered material is formed at high  $\text{Nd}_2\text{O}_3$  concentration ( $>15$  wt.%). This critical concentration was also observed with  $\text{Al}_2\text{O}_3\text{-La}_2\text{O}_3$  materials prepared by the sol-gel method [24].

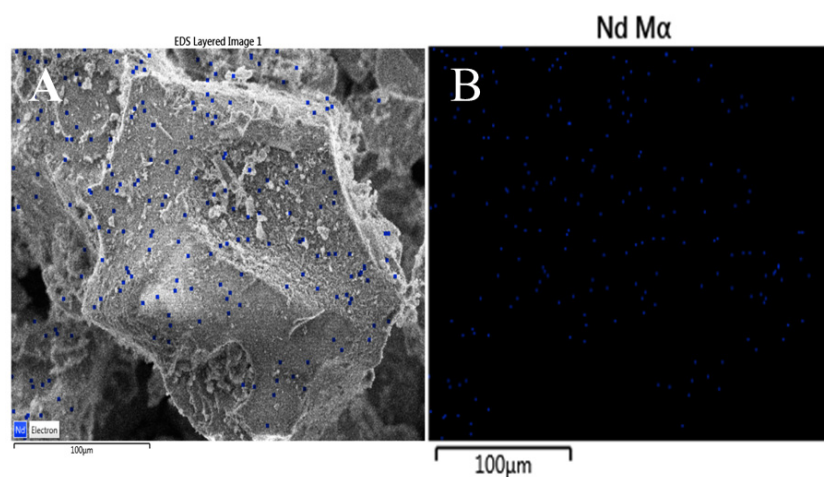


**Figure 4.** (A) EDS image of Al-Nd-15 binary oxide; (B) SEM mapping image of the element Nd  $M\alpha$  of the Al-Nd-15 binary oxide.

In order to get an insight into the morphology of the materials, SEM images of the  $\gamma\text{-Al}_2\text{O}_3$ , Al-Nd-15 and Al-Nd-25 binary oxides and  $\text{Nd}_2\text{O}_3$  are shown in Figure 5A–D. The SEM micrograph of  $\gamma\text{-Al}_2\text{O}_3$  exhibits a highly fibrous homogeneous material (Figure 5A). Meanwhile, the SEM micrograph of the Al-Nd-15 binary oxide shows a disordered material composed of alumina granular agglomerates of different sizes (Figure 5B). The morphology of the material changes at higher  $\text{Nd}_2\text{O}_3$  concentration and the SEM micrograph of Al-Nd-25 binary oxide (Figure 5C) displays the formation of pieces of calcareous hollow material of different sizes, while the SEM micrograph of bare  $\text{Nd}_2\text{O}_3$  depicts a highly crystalline material composed of plane layer agglomerates (Figure 5D).

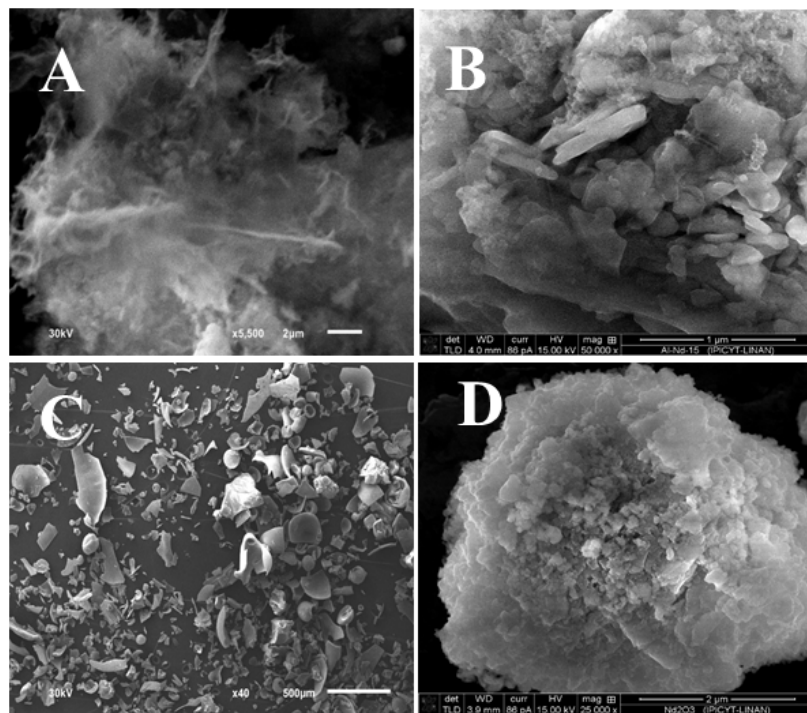


**Figure 5.** SEM micrographs of (A)  $\gamma$ - $\text{Al}_2\text{O}_3$ ; (B) Al-Nd-15; (C) Al-Nd-25; (D)  $\text{Nd}_2\text{O}_3$ .

A SEM mapping by element throughout an egg shell-type hollow spheroidal particle of the Al-Nd-25 binary oxide of Figure 5C indicates that aluminum and oxygen are compactly and evenly distributed, keeping the morphology of the particle (Figure 6), whereas neodymium is highly dispersed over the whole of the particle and carbon is densely populated throughout and outside of the particle. It is inferred that a high  $\text{Nd}_2\text{O}_3$  concentration in the binary oxide, the calcination temperature, and the residual carbon from the 2,4-pentaneodiol used as a chemical modifier during the synthesis of the materials by the sol-gel method might result in different morphologies of the particles, in particular the residual carbon from the 2,4-pentaneodiol might act as a template giving rise to the framework of the hollow spheroidal particles.

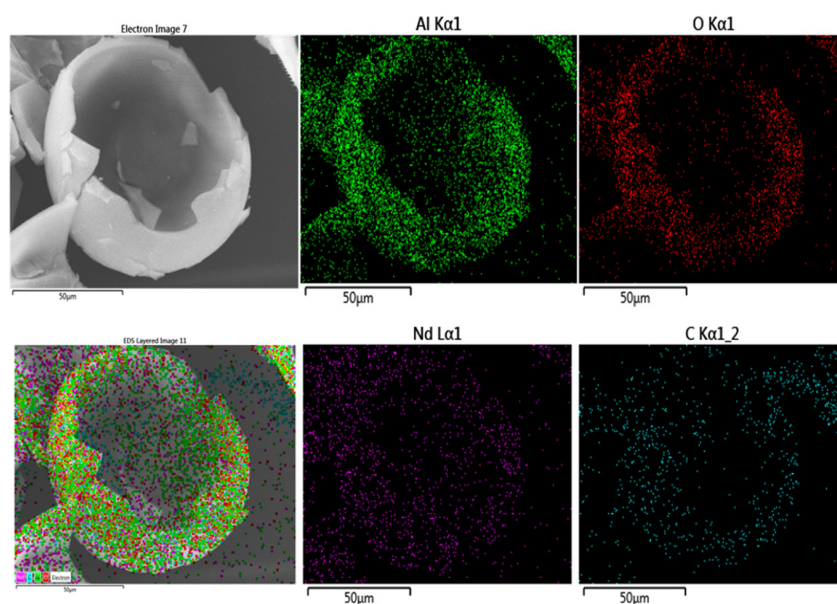


**Figure 6.** SEM mapping image by element of the Al-Nd-25 binary oxide.

### 3.3. Band Gap Energy of $\text{Al}_2\text{O}_3$ - $\text{Nd}_2\text{O}_3$ Binary Oxides

The UV-Vis spectra of the  $\gamma$ - $\text{Al}_2\text{O}_3$  and  $\text{Nd}_2\text{O}_3$  references as well as the Al-Nd- $x$  binary oxides are shown in Figure 7. The spectrum of  $\gamma$ - $\text{Al}_2\text{O}_3$  presented a broad absorption in the 240–330 nm range, which is associated with electronic charge transfer and also with the accumulation of defects in the structure of this compound [25]. Regarding the  $\text{Nd}_2\text{O}_3$  sample, the spectrum contains an intense band in the 200–290 nm range associated with an exchange of electrons between the valence and conduction bands [9,26]; also, a set of sharp absorption bands between 330 and 760 nm correspond to electron transitions within the 4f shell of neodymium [3,27].

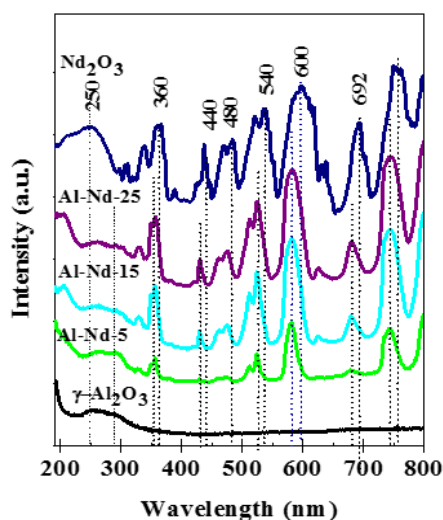


Figure 7. UV-Vis spectra of  $\gamma$ - $\text{Al}_2\text{O}_3$ , Al-Nd- $x$  binary oxides and  $\text{Nd}_2\text{O}_3$ .

Regarding the spectra of the binary oxides, the band between 240 and 315 nm from the alumina is present. In contrast, the intense and narrow absorption bands between 320 and 740 nm due to internal transitions in  $\text{Nd}^{3+}$  are slightly shifted to lower wavelengths due to a chemical interaction between  $\text{Nd}_2\text{O}_3$  and  $\gamma$ - $\text{Al}_2\text{O}_3$  phases [9,27,28]. The absorption band in the UV region of pristine  $\text{Nd}_2\text{O}_3$  was used to determine the band gap energy ( $E_g$ ) in the mixed oxides as these signals are produced by transference of electrons between the valence and conduction bands [9,26,29] and because this band is clearly defined in all the spectra and it is overlapped with the absorption band of  $\gamma$ - $\text{Al}_2\text{O}_3$ . The plots to determine the  $E_g$  according to the Tauc equation [20] are depicted in Figure S1, whereas the  $E_g$  values are shown in Table 1.

Table 1. Band gap energy of  $\text{Al}_2\text{O}_3$ - $\text{Nd}_2\text{O}_3$  binary oxides prepared by the sol-gel method.

Material	Band Gap Energy (eV)
$\gamma$ - $\text{Al}_2\text{O}_3$	3.35
Al-Nd-5	3.54
Al-Nd-10	3.20
Al-Nd-15	3.13
Al-Nd-25	3.19
$\text{Nd}_2\text{O}_3$	3.98

The band gap energy value of  $\gamma$ - $\text{Al}_2\text{O}_3$  ( $E_g = 3.35$  eV) is by far lower than that reported for insulators ( $>5$  eV) [1–3]. The low  $E_g$  value of  $\gamma$ - $\text{Al}_2\text{O}_3$  might be due to surface defects concentration in the  $\gamma$ - $\text{Al}_2\text{O}_3$  particles. This can be correlated with the increase in the hybridization of the  $\text{SP}^3$  orbitals of  $\gamma$ - $\text{Al}_2\text{O}_3$  [4]. Compared with the  $E_g$  value of  $\gamma$ - $\text{Al}_2\text{O}_3$ , the  $E_g$  of Al-Nd-5 binary oxide increases

to 3.54 eV probably due to the presence of highly dispersed  $\text{Nd}_2\text{O}_3$  nanoparticles, whereas the  $E_g$  of the binary oxides decreases to a minimum value ( $E_g = 3.13$  eV) at higher  $\text{Nd}_2\text{O}_3$  concentration, as observed in the Al-Nd-15 sample with  $E_g = 3.13$  eV. The band gap energies of the oxides with  $\text{Nd}_2\text{O}_3$  concentration between 10 and 25 wt.% were between 3.13 and 3.20 eV, and these are typical of semiconducting materials absorbing in the UV region. The calculated band gap energy value for pristine  $\text{Nd}_2\text{O}_3$  ( $E_g = 3.8$  eV) corresponds to electronic transitions between the valence and conduction bands [30,31]. The lower  $E_g$  values of the binary oxides suggest the use as photocatalysts. In particular, the low  $E_g$  values of binary oxides with  $\text{Nd}_2\text{O}_3$  concentrations between 10 and 25 wt.% could be explained by the overlap of electronic bands from  $\gamma\text{-Al}_2\text{O}_3$  and  $\text{Nd}_2\text{O}_3$ . This is suggested because the absorption bands of “4f<sup>3</sup>” transitions in the UV-Vis spectra of pristine  $\text{Nd}_2\text{O}_3$  are shifted to lower wavelengths for approximately 13–20 nm in the UV-Vis spectra of Al-Nd-*x* binary oxides (Figure 6), indicating that  $\text{Nd}_2\text{O}_3$  species are chemically interacting with  $\gamma\text{-Al}_2\text{O}_3$ . Such interaction between  $\gamma\text{-Al}_2\text{O}_3$  and  $\text{Nd}_2\text{O}_3$  might be facilitated by the sol-gel preparation method since the compounds are well-mixed and thus promote an easier interaction between species.

#### 3.4. Photocatalytic Activity of $\text{Al}_2\text{O}_3\text{-Nd}_2\text{O}_3$ Binary Oxides in the Degradation of Diclofenac

The photocatalytic activity of  $\gamma\text{-Al}_2\text{O}_3$ ,  $\text{Nd}_2\text{O}_3$  and the binary oxides was evaluated in the degradation of diclofenac solutions with concentrations of 80 ppm. Previous to the photocatalytic experiments, the diclofenac solution was submitted to UV light irradiation without the use of any photocatalyst (Figure 8).

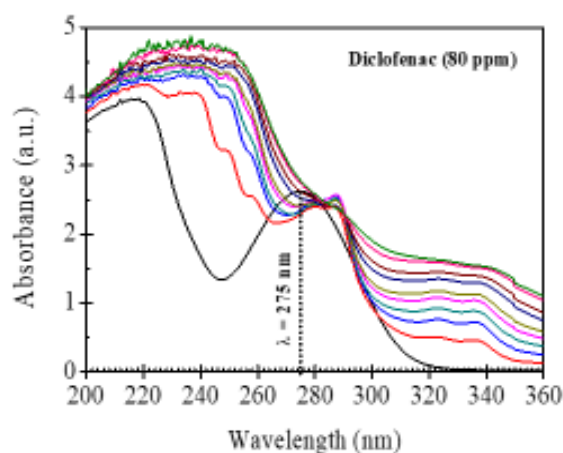


**Figure 8.** Photolysis of diclofenac using UV light irradiation without any photocatalyst.

The UV-vis spectrum indicated the stability of the drug against UV radiation; only the intensity of the band around 275 nm was slightly reduced. This band corresponds to electronic transitions of substituent groups in the diclofenac molecules, while the aromatic moiety of diclofenac is retained in the absence of a photocatalyst. The UV-Vis spectra of diclofenac after irradiation with UV light using  $\gamma\text{-Al}_2\text{O}_3$  during a period of 80 min show that the intensity of the absorption band located at 275 nm decreases with the irradiation time and completely disappears after 60 min of UV light irradiation (Figure 9A), indicating the total degradation of diclofenac molecules after this time. However, with the presence of neodymium in binary oxide, the absorption band located at 275 nm decreases more quickly with the photoreaction time and completely disappears after only 40 min of UV light irradiation, indicating a higher photodegradation of diclofenac (Figure 9B).



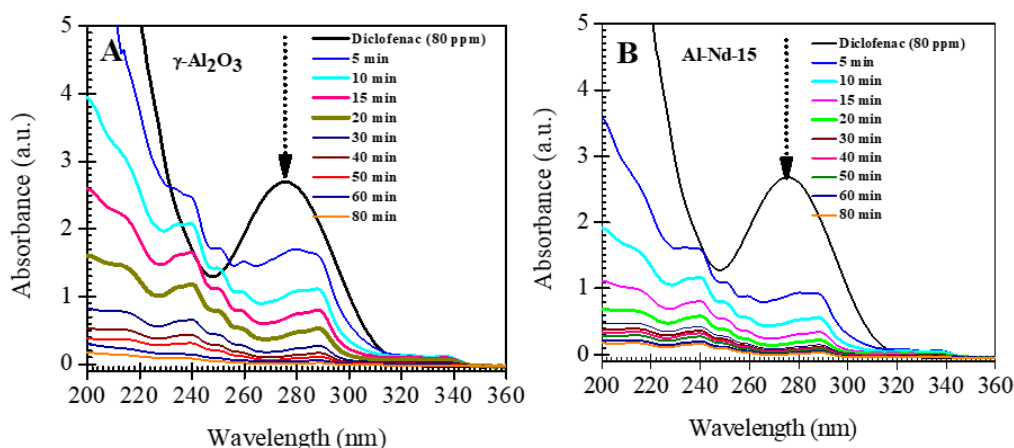


**Figure 9.** UV-Vis spectra of diclofenac after irradiation with UV light irradiation using: (A)  $\gamma\text{-Al}_2\text{O}_3$ ; (B) Al-Nd-15 binary oxide.

As shown in the upper plot of Figure 10, the adsorption percentage of diclofenac over Al-Nd-15 binary oxide using dark light after 80 min of exposure was less than 12%. Figure 10 also shows the relative concentration ( $C/C_0$ ) of diclofenac as a function of the photoreaction time after irradiation with UV light using  $\gamma\text{-Al}_2\text{O}_3$ , Al-Nd- $x$  and  $\text{Nd}_2\text{O}_3$  photocatalysts.  $\gamma\text{-Al}_2\text{O}_3$  and Al-Nd- $x$  binary oxides reach more than 92.0% of photoconverted diclofenac after 40 min of UV exposure. However, the relative concentration of diclofenac decreases more quickly with the  $\text{Nd}_2\text{O}_3$  concentration to reach the higher drop in the Al-Nd-15 binary oxide. The photoconversion of diclofenac using  $\gamma\text{-Al}_2\text{O}_3$  was 63.0% at 10 min of UV light exposure, whereas Al-Nd-15 binary oxide reached 82.0% at this photoreaction time. The photoconversion percentage of diclofenac at 10 min of photoreaction using Al-Nd-10 and Al-Nd-25 binary oxides was also improved with respect to that of  $\gamma\text{-Al}_2\text{O}_3$ , reaching diclofenac photoconversions of 69.0% and 78.0%, respectively. This means that the photocatalytic activity in the degradation of diclofenac using Al-Nd- $x$  binary oxides with  $\text{Nd}_2\text{O}_3$  contents in the range 10%–25% was improved with respect to that of  $\gamma\text{-Al}_2\text{O}_3$  at short photoreaction times. The photoconversion percentage using  $\text{Nd}_2\text{O}_3$  as a reference photocatalyst was lower than those of  $\gamma\text{-Al}_2\text{O}_3$  and Al-Nd- $x$  binary oxides, reaching 55.0% of photodegraded diclofenac after 10 min of UV light irradiation.

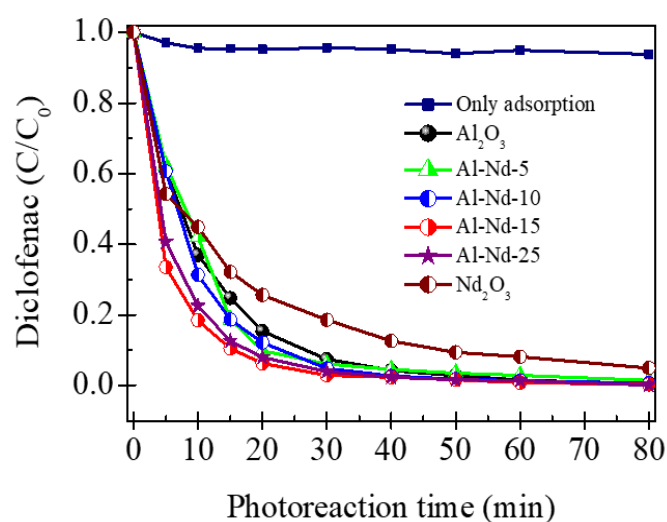


**Figure 10.** Relative concentration ( $C/C_0$ ) of diclofenac as a function of the photoreaction time using  $\gamma\text{-Al}_2\text{O}_3$ , Al-Nd- $x$  binary oxides, and  $\text{Nd}_2\text{O}_3$  as photocatalysts; inset plot represents the diclofenac adsorption with dark light over Al-Nd-15 binary oxide.

Kinetic Behavior of Al<sub>2</sub>O<sub>3</sub>-Nd<sub>2</sub>O<sub>3</sub> Binary Oxides in the Photodegradation of Diclofenac

The kinetic data from the photodegradation of diclofenac were plotted as  $\ln(C_0/C)$  versus reaction time ( $t$ ) (Figure 11). The linear plots obtained with  $\gamma$ -Al<sub>2</sub>O<sub>3</sub>, Nd<sub>2</sub>O<sub>3</sub>, and the binary oxide catalysts are evidence of the pseudo first-order kinetics of the Langmuir-Hinshelwood type. The kinetics are constant with the photodegradation of diclofenac over  $\gamma$ -Al<sub>2</sub>O<sub>3</sub> was  $7.9 \times 10^{-1} \text{ min}^{-1}$ , while the half-life time ( $\tau_{1/2}$ ) was 8.74 min (Table 2). In the binary oxides, the reaction rate constant ( $k$ ) increases with Nd<sub>2</sub>O<sub>3</sub> concentration to reach a maximum reaction rate constant ( $k = 9.5 \times 10^{-1}$ ) after 40 min of UV light irradiation and the half-life time decreases to a minimum ( $\tau_{1/2} = 7.32$  min). At higher Nd<sub>2</sub>O<sub>3</sub> concentration the reaction rate constant decreases to reach a  $k = 4.8 \times 10^{-1} \text{ min}^{-1}$  in the pristine Nd<sub>2</sub>O<sub>3</sub> photocatalyst.

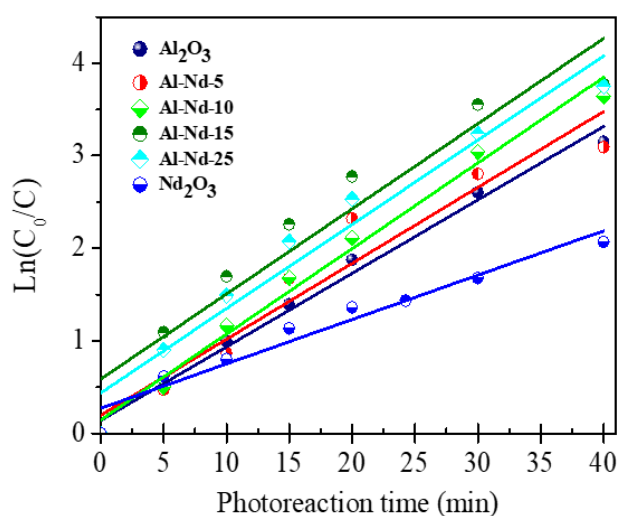


**Figure 11.**  $\ln(C_0/C)$  vs. photoreaction time ( $t$ ) after photodegradation of diclofenac using  $\gamma$ -Al<sub>2</sub>O<sub>3</sub>, Al-Nd- $x$  binary oxide and Nd<sub>2</sub>O<sub>3</sub>.

**Table 2.** Rate constant ( $k$ ) and half-life time ( $\tau_{1/2}$ ) in the diclofenac photo-degradation reaction using Al<sub>2</sub>O<sub>3</sub>-Nd<sub>2</sub>O<sub>3</sub> binary oxides.

Photocatalyst	$k \times 10^{-2} \text{ (min}^{-1}\text{)}$	$\tau_{1/2} \text{ (min)}$
Al <sub>2</sub> O <sub>3</sub>	7.9	8.74
Al-Nd-5	8.2	8.46
Al-Nd-10	9.3	7.50
Al-Nd-15	9.5	7.29
Al-Nd-25	9.1	7.61
Nd <sub>2</sub> O <sub>3</sub>	4.8	14.50

The kinetic studies confirm that Al<sub>2</sub>O<sub>3</sub>-Nd<sub>2</sub>O<sub>3</sub> with Nd<sub>2</sub>O<sub>3</sub> concentrations between 10 and 25 wt.% of Nd<sub>2</sub>O<sub>3</sub> presented the highest activity to degrade diclofenac since these compounds achieved higher reaction rate constants and lower half-life times (Table 2). The highest activity for the photoconversion of diclofenac with 10% and 25% of Nd<sub>2</sub>O<sub>3</sub> in the binary oxides correlates with their lower band gap energies.

### 3.5. Recombination Rate of Electron–Hole Pairs in the Binary Oxides

(PL) spectroscopy was used to evaluate the effect of the Nd<sub>2</sub>O<sub>3</sub> content in the binary oxides on the recombination rate of electron–hole. Figure 12 shows the PL spectra of the binary oxides and the  $\gamma$ -Al<sub>2</sub>O<sub>3</sub> and Nd<sub>2</sub>O<sub>3</sub> references. The intensity of the PL spectra of Al-Nd-5 increased with respect to

that of  $\gamma$ -Al<sub>2</sub>O<sub>3</sub>, indicating a higher recombination rate which is close to the values of the reference Nd<sub>2</sub>O<sub>3</sub>. The intensity produced by the Al-Nd-10 sample maintained that of the  $\gamma$ -Al<sub>2</sub>O<sub>3</sub> indicating lack of enhancement in the recombination rate. However, at higher Nd<sub>2</sub>O<sub>3</sub> concentration ( $\geq 15$  wt.%) the intensity decreased when the content of Nd<sub>2</sub>O<sub>3</sub> increased suggesting that Nd<sub>2</sub>O<sub>3</sub> acts as a separator of electron-hole pairs and favors the improvement in the photocatalytic activity.

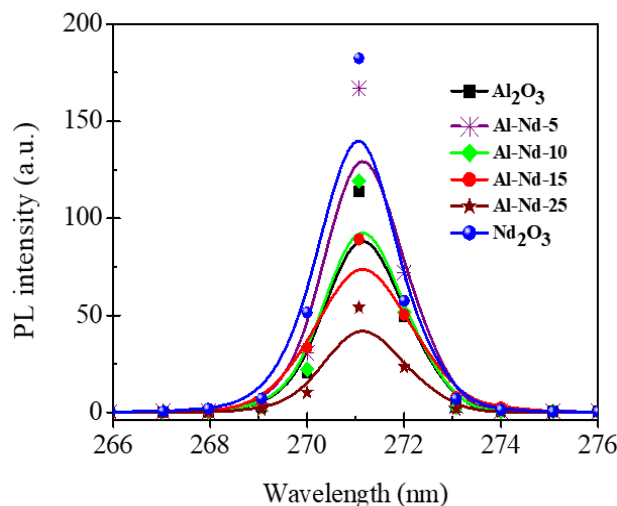


Figure 12. PL spectra of  $\gamma$ -Al<sub>2</sub>O<sub>3</sub>, Al-Nd-*x* binary oxides and Nd<sub>2</sub>O<sub>3</sub>.

#### 4. Conclusions

The photocatalytic activity of the Al<sub>2</sub>O<sub>3</sub>-Nd<sub>2</sub>O<sub>3</sub> binary oxides was evaluated and compared with isolated Al<sub>2</sub>O<sub>3</sub> and Nd<sub>2</sub>O<sub>3</sub> references. The relative concentration of diclofenac catalyzed with  $\gamma$ -Al<sub>2</sub>O<sub>3</sub> and Al-Nd-*x* binary oxides decreased with the reaction time, reaching 92.0% of degradation after 30 min of reaction. However, the relative concentration of diclofenac decreased faster when catalyzed with Al-Nd-*x* binary oxides for Nd<sub>2</sub>O<sub>3</sub> contents between 10 and 25 wt.%, reaching diclofenac photoconversions between 88.0% and 94.0% after only 10 min of photoreaction. Additionally, the kinetic studies confirm that the highest activity was reached with Al-Nd-*x* binary oxides with Nd<sub>2</sub>O<sub>3</sub> concentrations of 15 and 25 wt.%. The highest activity is correlated with the lower band gap energies found in these materials, resulting from the defects concentration within the Al<sub>2</sub>O<sub>3</sub> matrix. These low energies, along with the low recombination rates of electron-hole pairs enhanced by the Nd<sub>2</sub>O<sub>3</sub> crystalline domains, provide evidence that the Al<sub>2</sub>O<sub>3</sub>-Nd<sub>2</sub>O<sub>3</sub> binary oxides are suitable photocatalysts for degradation of organic compounds, especially diclofenac which is a persistent pollutant.

**Supplementary Materials:** The following are available online at <http://www.mdpi.com/1996-1944/13/6/1345/s1>, Figure S1:  $(\alpha h\nu)^2$  vs. Energy plot for the calculation of the band gap energy of Al-Nd-*x* binary oxides prepared by the sol-gel method.

**Author Contributions:** Conceptualization, A.B. and F.T.; methodology, J.E.C. and A.L.-G.; formal analysis, J.C.-M. and S.U.-G.; investigation, A.B. and F.T.; writing—original draft preparation, J.E.C. and A.B.; writing—review and editing, A.B.; visualization, A.B. and M.E.C.; supervision, F.T. and G.G.C.A. All authors have read and agreed to the published version of the manuscript.

**Funding:** This work was partially supported by grants from COECYTJAL (Project: 06-200732), CONACYT (Projects: 119058, 169157 and 154994), PROSNI and PRODEP. J. E. Casillas is indebted to CONACYT for granting a scholarship (CONACYT scholar No. 287873).

**Acknowledgments:** The authors thanks to M in Sci. Ana Iris Peña Maldonado of IPICYT for the technical assistance of HSEM measurements.

**Conflicts of Interest:** The authors declare no conflict of interest.

## References

1. Shin, B.; Weber, J.R.; Long, R.D.; Hurley, P.K.; Van de Walle, C.G.; MacIntyre, P.C. Origin and passivation of fixed charge in atomic layer deposited aluminum oxide gate insulators on chemically treated InGaAs substrates. *Appl. Phys. Lett.* **2010**, *96*, 152908. [[CrossRef](#)]
2. Price, J.; Bersuker, G.; Lysaght, P.S. Identification of interfacial defects in high-k gate stack films by spectroscopic ellipsometry. *J. Vac. Sci. Technol. B* **2009**, *27*, 310–312. [[CrossRef](#)]
3. French, R.A. Electronic band structure of Al<sub>2</sub>O<sub>3</sub>, with comparison to Alon and AlN. *J. Am. Ceram. Soc.* **1990**, *73*, 477–489. [[CrossRef](#)]
4. Ealet, B.; Elyakhloufi, M.H.; Gillet, E.; Ricci, M. Electronic and crystallographic structure of  $\gamma$ -alumina thin films. *Thin Solid Films* **1994**, *250*, 92–100. [[CrossRef](#)]
5. Mullins, W.M.; Averbach, B.L. The electronic structure of anodized and etched aluminum alloy surfaces. *Surf. Sci.* **1988**, *206*, 52–60. [[CrossRef](#)]
6. Mullins, W.M. The effect of Fermi energy on reaction of water with oxide surfaces. *Surf. Sci.* **1989**, *217*, 459–467. [[CrossRef](#)]
7. Tzompantzi, F.; Piña, Y.; Mantilla, A.; Aguilar-Martinez, O.; Galindo-Hernández, F.; Bokhimi, X.; Barrera, A. Hydroxylated sol-gel Al<sub>2</sub>O<sub>3</sub> as photocatalyst for the degradation of phenolic compounds in presence of UV light. *Catal. Today* **2014**, *220–222*, 49–55. [[CrossRef](#)]
8. Barrera, A.; Tzompantzi, F.; Campa-Molina, J.; Casillas, J.E.; Pérez-Hernández, R.; Ulloa-Godinez, S.; Velásquez, C.; Arenas-Alatorre, J. Photocatalytic activity of Ag/Al<sub>2</sub>O<sub>3</sub>-Gd<sub>2</sub>O<sub>3</sub> photocatalysts prepared by the sol-gel method in the degradation of 4-chlorophenol. *RSC Adv.* **2018**, *8*, 3108–3119. [[CrossRef](#)]
9. Casillas, J.E.; Tzompantzi, F.; Castellanos, S.G.; Mendoza-Damián, G.; Pérez-Hernández, R.; López-Gaona, A.; Barrera, A. Promotion effect of ZnO on the photocatalytic activity of coupled Al<sub>2</sub>O<sub>3</sub>-Nd<sub>2</sub>O<sub>3</sub>-ZnO composites prepared by the sol-gel method in the degradation of phenol. *Appl. Catal. B Environ.* **2017**, *208*, 161–170. [[CrossRef](#)]
10. Barrera, A.; Tzompantzi, F.; Padilla, J.M.; Casillas, J.E.; Jacome-Acatitla, G.; Cano, M.E.; Gomez, R. Reusable PdO/Al<sub>2</sub>O<sub>3</sub>-Nd<sub>2</sub>O<sub>3</sub> photocatalysts in the UV photodegradation of phenol. *Appl. Catal. B Environ.* **2014**, *144*, 362–368. [[CrossRef](#)]
11. Barrera, A.; Tzompantzi, F.; Lara, V.; Gómez, R. Photodegradation of 2,4-D over PdO/Al<sub>2</sub>O<sub>3</sub>-Nd<sub>2</sub>O<sub>3</sub> photocatalysts prepared by the sol-gel method. *J. Photochem. Photobiol. A Chem.* **2012**, *227*, 45–50. [[CrossRef](#)]
12. Cordero-García, A.; Turnes Palomino, G.; Hinojosa-Reyes, L.; Guzmán-Mar, J.L.; Maya-Teviño, L.; Hernández-Ramírez, A. Photocatalytic behaviour of WO<sub>3</sub>/TiO<sub>2</sub>-N for diclofenac degradation using simulated solar radiation as an activation source. *Environ. Sci. Pollut. Res.* **2017**, *24*, 4613–4624. [[CrossRef](#)] [[PubMed](#)]
13. Mugunthan, M.; Saidutta, M.B.; Jagadeeshbabu, P.E. Photocatalytic degradation of diclofenac using TiO<sub>2</sub>-SnO<sub>2</sub> mixed oxide catalysts. *Environ. Technol.* **2019**, *40*, 929–941. [[CrossRef](#)] [[PubMed](#)]
14. Zhang, W.; Zhou, L.; Shi, J.; Deng, H. Synthesis of Ag<sub>3</sub>PO<sub>4</sub>/G-C<sub>3</sub>N<sub>4</sub> composite with enhanced photocatalytic performance for the photodegradation of diclofenac under visible light irradiation. *Catalysts* **2018**, *8*, 45. [[CrossRef](#)]
15. Bojanowska-Czajka, A.; Kciuk, G.; Gumiela, M.; Borowiecka, S.; Nałęcz-Jawecki, G.; Koc, A.; Garcia-Reyes, J.F.; Ozbay, D.S.; Trojanowicz, M. Analytical, toxicological and kinetic investigation of decomposition of the drug diclofenac in waters and wastes using gamma radiation. *Environ. Sci. Pollut. Res.* **2015**, *22*, 20255–20270. [[CrossRef](#)]
16. Khatem, R.; Miguel, R.O.; Bakhti, A. Use of synthetic clay for removal of diclofenac anti-inflammatory. *Eur. J. Soil Sci.* **2015**, *4*, 126–136. [[CrossRef](#)]
17. Zhang, W.; Zhou, L.; Deng, H. Ag modified g-C<sub>3</sub>N<sub>4</sub> composites with enhanced visible-light photocatalytic activity for diclofenac degradation. *J. Mol. Catal. A Chem.* **2016**, *423*, 270–276. [[CrossRef](#)]
18. Valente, J.S.; Tzompantzi, F.; Prince, J.; Cortez, J.G.H.; Gomez, R. Adsorption and photocatalytic degradation of phenol and 2,4 dichlorophenoxyacetic acid by Mg-Zn-Al layered double hydroxides. *Appl. Catal. B* **2009**, *90*, 330–338. [[CrossRef](#)]
19. Pavia, D.L.; Lampman, G.M.; Kriz, G.S. *Introduction to Spectroscopy*, 4th ed.; Cengage Learning: Washington, DC, USA, 2009.

20. Padhye, P.; Poddar, P. Static and dynamic photoluminescence and photocatalytic properties of uniform, monodispersed up/down-converting, highly luminescent, lanthanide-ion-doped  $\beta$ -NaYF<sub>4</sub> phosphor microcrystals with controlled multiform morphologies. *J. Mater. Chem. A* **2014**, *45*, 19189–19200. [[CrossRef](#)]
21. Sobczynski, A.; Duczmal, L.; Zmudzinski, W. Phenol destruction by photocatalysis on TiO<sub>2</sub>: An attempt to solve the reaction mechanism. *J. Mol. Catal. A Chem.* **2004**, *213*, 225–230. [[CrossRef](#)]
22. Kumar, K.V.; Porkodi, K. Comments on “Photocatalytic properties of TiO<sub>2</sub> modified with platinum and silver nanoparticles in the degradation of oxalic acid in aqueous solution” Langmuir Hinshelwood kinetics—A theoretical study. *Appl. Catal. B* **2008**, *79*, 108–109. [[CrossRef](#)]
23. Zhang, N.; Yi, R.; Zhou, L.; Gao, G.; Shi, R.; Qiu, G.; Liu, X. Lanthanide hydroxide nanorods and their thermal decomposition to lanthanide oxide nanorods. *Mater. Chem. Phys.* **2009**, *114*, 160–167. [[CrossRef](#)]
24. Barrera, A.; Fuentes, S.; Viniegra, M.; Borja, M.A.; Bogdanchikova, N.; Campa-Molina, J. Structural properties of Al<sub>2</sub>O<sub>3</sub>-La<sub>2</sub>O<sub>3</sub> binary oxides prepared by the sol-gel method. *Mater. Res. Bull.* **2007**, *42*, 640–648. [[CrossRef](#)]
25. Pérez Osorio, G.; Fuentes Moyado, S.; Petranovskii, V.; Simakov, A. PdO/Al<sub>2</sub>O<sub>3</sub>-(Ce<sub>1-X</sub>Zr<sub>X</sub>)O<sub>2</sub> catalysts: Effect of the sol-gel support composition. *Catal. Lett.* **2006**, *110*, 53–60. [[CrossRef](#)]
26. Umesh, B.; Eraiah, B.; Nagabhushana, H.; Nagabhushana, B.M.; Nagaraja, G.; Shivakumara, C.; Chakradhar, R.P.S. Synthesis and characterization of spherical and rod like nanocrystalline Nd<sub>2</sub>O<sub>3</sub> phosphors. *J. Alloy. Compd.* **2011**, *509*, 1146–1151. [[CrossRef](#)]
27. Caro, P. *Structure Electronique des Elements de Transition*, 1st ed.; Presses Universitaires de France: Paris, France, 1976.
28. Yuvakkumar, R.; Hong, S.I. Nd<sub>2</sub>O<sub>3</sub>: Novel synthesis and characterization. *J. Sol. Gel Sci. Technol.* **2015**, *73*, 511–517. [[CrossRef](#)]
29. Pan, L.K.; Chang, Q.S.; Li, C.M. Elucidating Si-Si dimer vibration from the size-dependent Raman shift of nanosolid Si. *J. Phys. Chem. B* **2004**, *108*, 3404–3406. [[CrossRef](#)]
30. Scarel, G.; Svane, A.; Fanciulli, M. Scientific and technological issues related to rare earth oxides. Rare Earth oxide thin films: Growth, characterization, and applications. In *Topics in Applied Physics*; Scarel, G., Fanciulli, M., Eds.; Springer: Berlin/Heidelberg, Germany, 2007; Volume 106.
31. Petit, L.; Svane, A.; Szotek, Z.; Temmerman, W.M. First principles study of rare-earth oxides. *Phys. Rev. B* **2005**, *72*. [[CrossRef](#)]



© 2020 by the authors. Licensee MDPI, Basel, Switzerland. This article is an open access article distributed under the terms and conditions of the Creative Commons Attribution (CC BY) license (<http://creativecommons.org/licenses/by/4.0/>).